

Experience with Use of Heavy W Shapes in Tension

JOHN W. FISHER and ALAN W. PENSE

During the last five years, a few cracking and fracture problems have been observed with welded, large rolled jumbo sections. This type of rolled section is classified as a group IV or V shape in the 8th Edition AISC *Manual of Steel Construction*.¹ They include W12 and W14 rolled steel sections equal or exceeding 210 lbs./ft. The cracking has been observed in sections equal or exceeding 370 lbs./ft. They have been observed in sections produced without special metallurgical requirements as well as in sections produced with killed fine grain practice. This paper reviews the characteristics of these steel sections, the conditions that led to the cracking and provides recommendations for splicing and use of these members in tension applications. In addition, there are suggestions for weld splices in compression.

When first introduced in the 1960s, these sections were intended as columns in structures resisting large axial loads. However, with passage of time the sections were gradually introduced in large trusses as tension members. This provided a means to develop the large forces in the chords and diagonals of long-span trusses or shorter spans carrying heavier loads. Figure 1 shows the fractured chord of a large truss fabricated from these rolled sections.

The cracks that developed have all been associated with groove welded splices in the flanges and webs of the steel sections. In the fracture shown in Fig. 2, the crack originated from the flame-cut copes in the web adjacent to the flange groove welds and extended into the web-flange core (i.e. the web-to-flange intersection). Other cracks have originated from the termination of groove welds in the web,



Fig. 1. Fractured chord of Orlando Civic Center truss

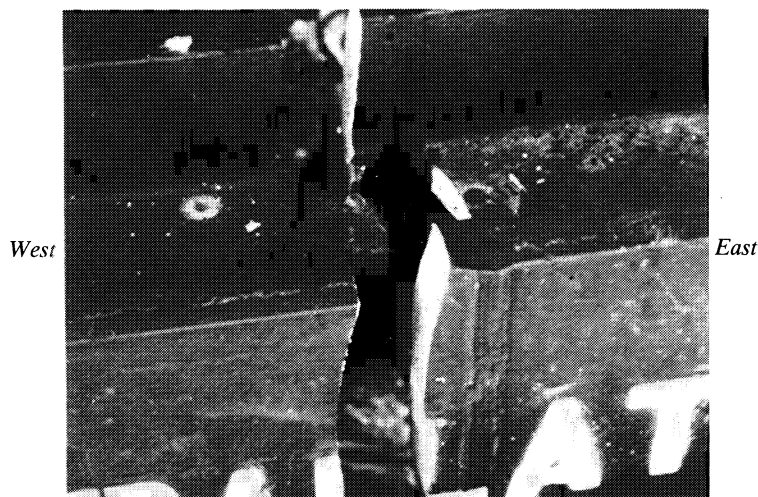


Fig. 2. Close-up of fracture

Dr. John W. Fisher is Professor of Civil Engineering at Lehigh University.

Dr. Alan W. Pense is Professor of Lehigh University's Department of Materials Science and Engineering, and Associate Dean in the College of Engineering and Physical Sciences.

as in Fig. 3 or from the groove welded web splice, as in Fig. 4. Cracks also developed from the flame-cut ends of large sections and extended a short distance longitudinally into the section, as in Fig. 5. The causes for each of these cracking conditions is examined in this paper along with recommendations for their correction.

DETAILS AND CHARACTERISTICS AT CRACKED SECTIONS

a. Fractured Tension Chord

The fracture in the bottom chord of the truss shown in Figs. 1 and 2 originated from a crack formed from the flame-cut surface of the web cope hole in a W14 × 370 A572 Gr.50 steel section. Figure 6 shows the fracture surface and a closeup view of the crack origin. The dark oxide-covered surface extends 1.15 in. from the edge of the cope into the flange; its maximum width 2.75 in. At the other end of the web cope, no obvious cracking was visible, as shown in Fig. 7. This area was saw-cut from the section and the flame-cut

surface treated with liquid penetrant, as seen in Fig. 8. This revealed a crack-like indication. No evidence of cracking was found on either outside surface of the web of this detail.

The cope segment was cut into two pieces by sawing at the mid-thickness of the web. This surface was polished and etched as in Fig. 9 which shows the crack originated at the flame-cut edge and extended on an angle into the web-flange core. Figure 10 shows the saw-cut surface of the section where the web was cut from the flange. This crack was found to extend into the flange about the same amount observed at the dark oxide surface in Fig. 6. A martensitic layer can be seen along the flame-cut edge in Fig. 9. A photomicrograph of the crack origin is provided in Fig. 11. The martensitic layer is about 0.025 in. thick. At the crack, the martensite Rockwell hardness (R_c) was 42.5 and varied between 32 and 37 elsewhere along the burned edge.

An examination of other flame-cut copes in W14 × 455 and W14 × 500 sections in the structure revealed other cracks, as in Fig. 12. At the section that failed, the web-groove weld was made first, followed by the outside halves

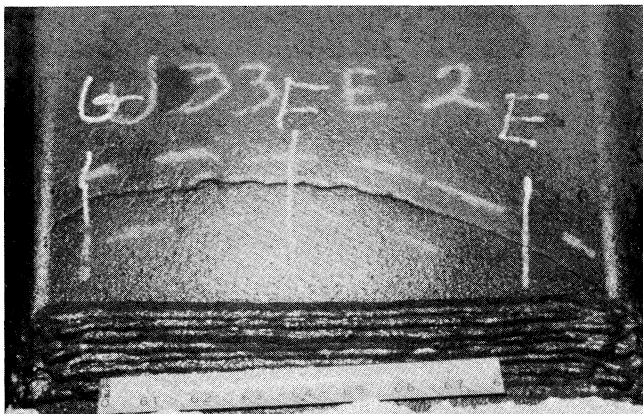
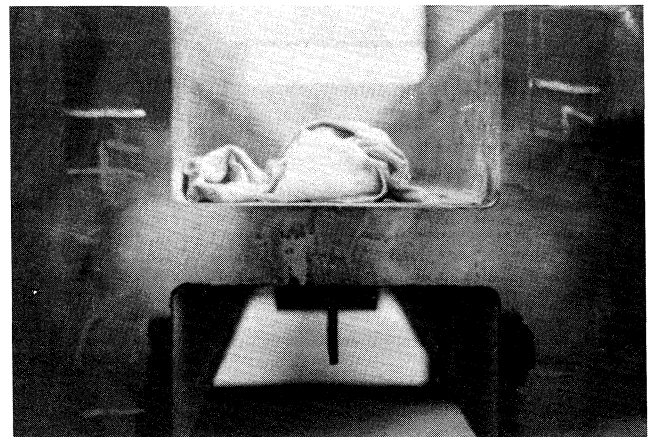


Fig. 3. Cracked column web originating at groove-welded web splice termination



(a). Milled end of column at splice

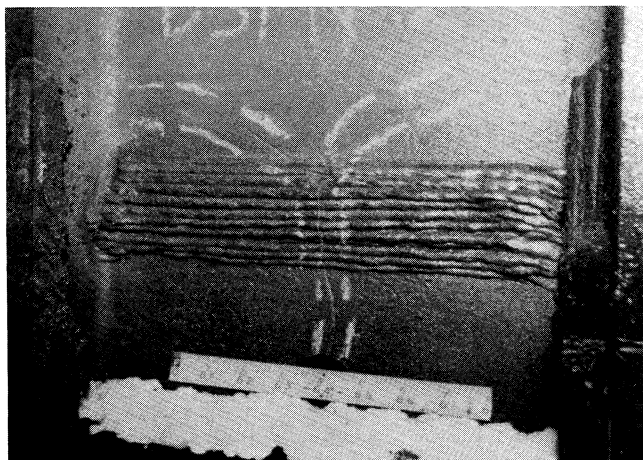
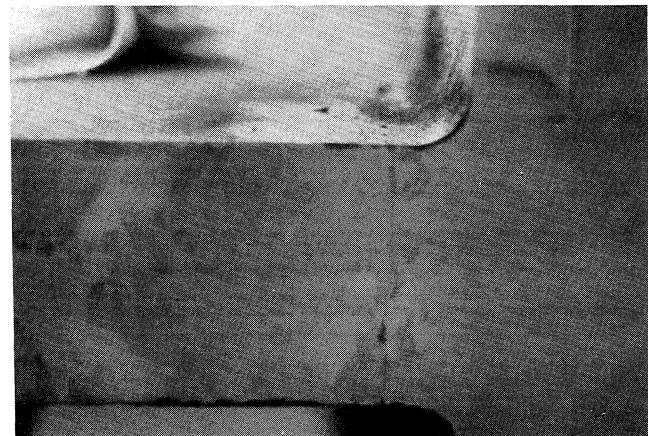


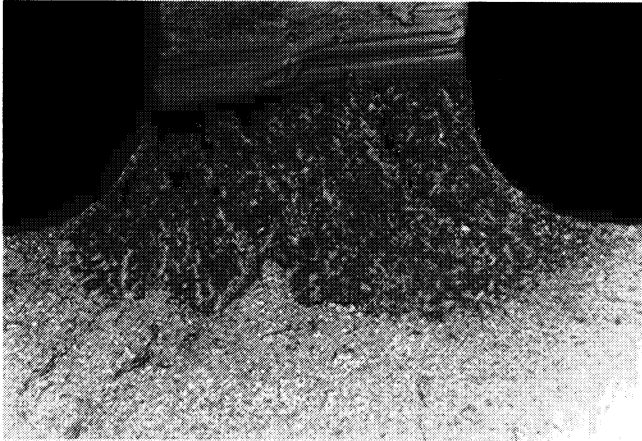
Fig. 4. Cracked column web originating at groove weld



(b). Longitudinal crack in web
Fig. 5. Crack originating from flame-cut edge



(a). Fracture surface of flange



S.W. fracture surface

(b). Close-up view of initial crack at web cope

Fig. 6. Crack surface of tension chord (see Fig. 1.)

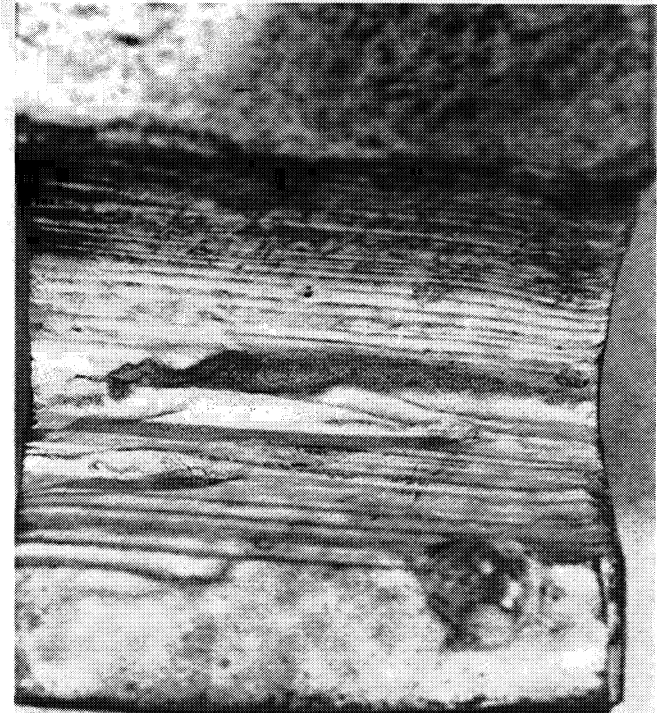


Fig. 8. Flame-cut cope with liquid penetrant



Fig. 7. Cope on east side of flange-groove weld (see Fig. 2.)

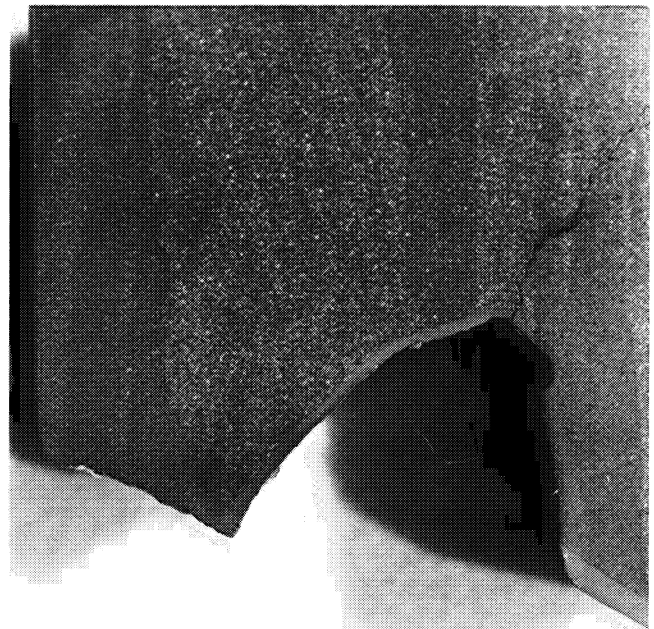


Fig. 9. Polished and etched section through center of web (see Fig. 8.) showing crack and flame cut edge

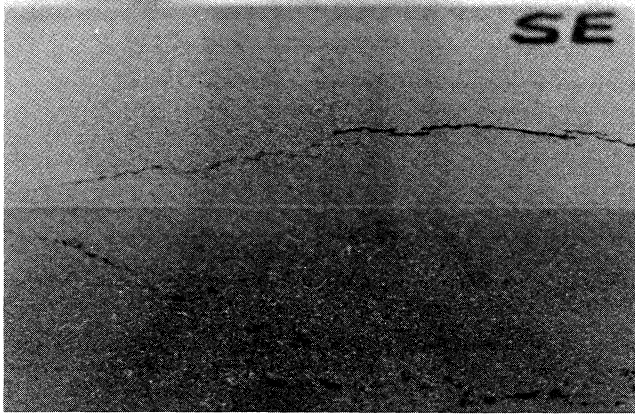


Fig. 10. Liquid penetrant indication showing crack extension into web-flange core

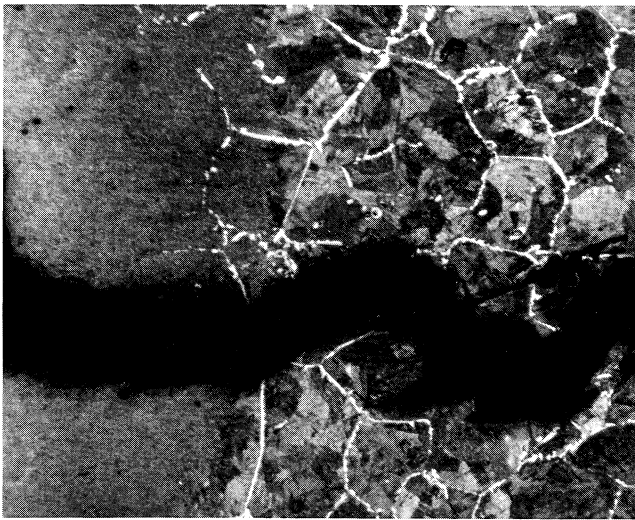


Fig. 11. Photomicrograph showing crack martensite and grain structure @ 40x

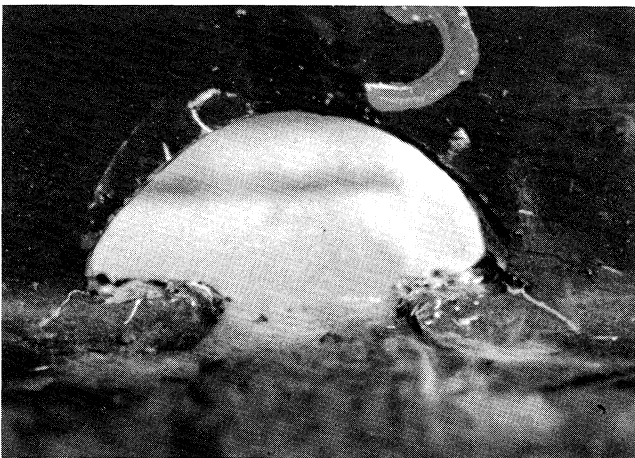


Fig. 12. Crack indications at cope enhanced by magnetic particle

of the flange double bevel groove welds. The inside weld halves of the flanges were completed last. At other sections that were field-welded, the flange groove welds were made first and the web groove weld last. In a number of the sections welded in this latter fashion, cracks developed in the web from the flame-cut edge of the cope. Nearly all welded splice locations had cracks at the cope, as in Fig. 12, which did not appear to depend on the weld sequence. The rolled sections in these truss members were all A572 Gr.50 steel material. They had not been supplied as killed, fine-grain practice steel sections.

b. Groove Welded Column Splices

The cracks that originated from the web groove weld termination shown in Fig. 3 occurred in W14 x 730 A572 Gr.50 steel sections. However, this material was supplied as killed, fine-grain practice steel. Figure 13 shows a schematic of the column splice at the cracked section. Partial penetration welds were placed in the flange and a double bevel groove weld in the web. At the weld ends, the bevel was radiused to the surface. Production of the web groove welds creates high tensile residual stresses in the longitudinal and transverse directions of the weld as it shrinks and cools. As a result, the weld termination resides in a region of yield point residual tensile stress in the web of the rolled section.

The cracks developed in these sections occurred even when preheat and postheat treatments were used. At the time cracks formed, ambient temperature was between 25 and 40° F. The crack shown in Fig. 4 likely occurred from an embedded defect on the fusion line of the rolled section. No core was removed at the crack origin so this was not verified by examination.

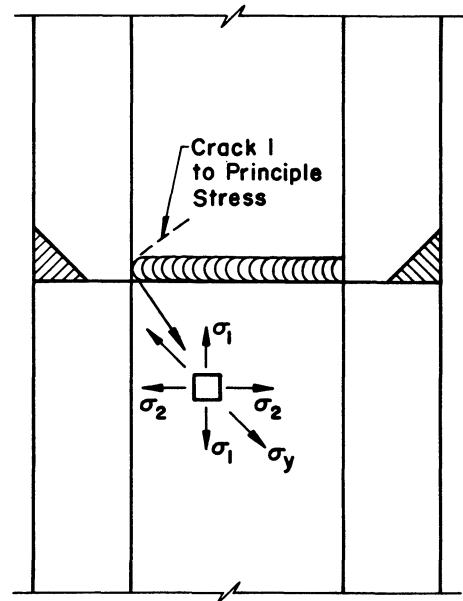


Fig. 13. Schematic showing joint geometry, residual stress orientation and crack

c. Longitudinal Cracks at Flame-Cut Edges

The cracks detected in the milled end of the column in Fig. 5 were observed to form from the flame-cut edge. These cracks extended about $\frac{3}{4}$ in. into the length direction of the section. These columns were also W14 \times 730 A572 Gr.50 steel sections. As apparent from Fig. 11, a thin martensitic layer can be expected at the flame-cut edge. Also, residual tensile surface stresses will develop as the cut is made and the material transforms from a liquid to solid state and cools. Measurements have demonstrated that yield point residual stresses will develop at a flame-cut edge.²

CHARACTERISTICS OF THE JUMBO SECTIONS

The material properties of the fractured and cracked sections shown in Figs. 1, 3 and 7 will be examined together with additional tests on several large sections that have been recently evaluated. This includes their tensile properties, microstructure, chemical composition and fracture characteristics (Charpy V-notch and fracture toughness tests).

a. Tensile Properties

The tensile tests of the two W14 \times 370 A572 Gr.50 steel sections adjacent to the fracture in Fig. 1 provided an average yield point of 61.3 ksi for the fractured section and 60.6 ksi for the adjacent one, with similar cracks in the flame-cut cope. The corresponding tensile strengths were 94.6 ksi and 91 ksi. The percent elongation in 2 in. varied from 20 to 26% and the reduction in area was about 55% for both sections.

For the W14 \times 730 A572 Gr.50 sections in Figs. 3 and 4, the yield point was 61.7 ksi, the tensile strength 86.1 ksi, and the elongation 29%. Additional tests carried out on the webs of W14 \times 550, W14 \times 605 and W14 \times 730 steel sections from a third supplier and manufactured to killed fine-grain practice had web-yield points between 54 and 58 ksi. These sections had similar tensile characteristics ranging between 87 and 92 ksi.

b. Chemical Analysis of Steel Sections

Chemical analyses were carried out on the W14 \times 370 sections from Supplier A that were taken from the cracked chord. The W14 \times 730 sections from Supplier B that experienced cracks at column groove welds were also tested. Tests were carried out on web samples from the W14 \times 550, W14 \times 605 and W14 \times 730 sections evaluated from Supplier C.

The test results are summarized in Table 1. When compared with the ASTM Specifications, it was found none of the elements were out of the specification limits for the applicable grade. For the fractured W14 \times 370 section, the carbon and manganese were near the upper limit and provided a carbon equivalent of at least 0.55. This indicated a high potential for cracking in heat-affected zone areas such as flame-cut edges and welds.

Table 1

| Chemical | W14 \times 370 | W14 \times 730 | W14 \times 550 | W14 \times 605 | W14 \times 730 |
|--------------|------------------------|----------------------|----------------------|----------------------|----------------------|
| | Core Supplier A* | Web Supplier B | Web Supplier C | Web Supplier C | Web Supplier C |
| Carbon | 0.22 | 0.18 | 0.27 | 0.25 | 0.24 |
| Manganese | 1.35 | 1.23 | 0.97 | 1.00 | 0.87 |
| Phosphorus | 0.01 | 0.022 | 0.028 | 0.025 | 0.017 |
| Sulfur | 0.022 | 0.014 | 0.040 | 0.032 | 0.027 |
| Silicon | <0.01 | 0.28 | 0.24 | 0.24 | 0.19 |
| Vanadium | 0.08 | 0.07 | 0.049 | 0.061 | 0.059 |
| Chromium | 0.103 | — | 0.078 | 0.077 | 0.079 |
| Nickel | 0.091 | — | 0.041 | 0.044 | 0.100 |
| Columbim(Nb) | <0.01 | 0.03 | — | — | — |
| Titanium | <0.01 | — | — | — | — |
| Copper | 0.028 | — | — | — | — |
| Aluminum | 0.003 | — | — | — | — |

*Not killed, fine-grain practice.

c. Charpy V-Notch Test Results

Charpy V-notch tests were carried out on the web and flange material of the fractured section shown in Fig. 2 (W14 \times 370). Tests were carried out at the standard quarter thickness locations in the web and flange, the web-flange core and the surface layers. Figure 14 shows a schematic with these locations. Orientation of the notch is indicated for the various specimen locations.

The test results are summarized in Fig. 15. The quarter thickness results are shown as plus (+), the web-flange core region and centerline as solid dots (•) and the surface layers as open dots (○). It can be seen the web-flange core and the flange quarter-point specimens provided comparable levels of absorbed energy up to 130° F. The quarter thickness web specimens were similar to the flange-web core below 100° F. However, at and above 100° F, web specimens tended to exhibit higher levels of energy and scatter.

The surface specimens with notches within 0.2 in. of the surface all provided significantly higher levels of absorbed

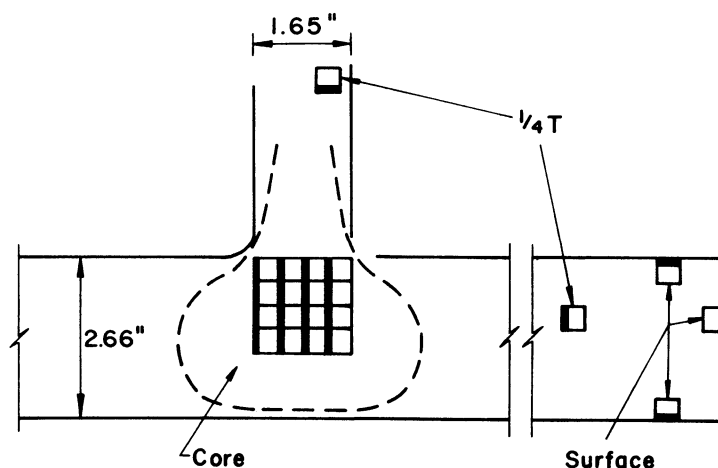


Fig. 14. Schematic showing CVN test locations for W14 \times 370 section—Supplier A

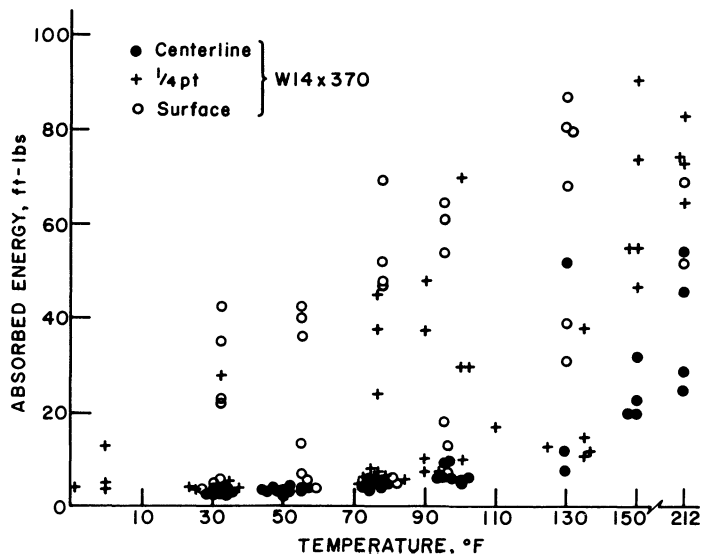


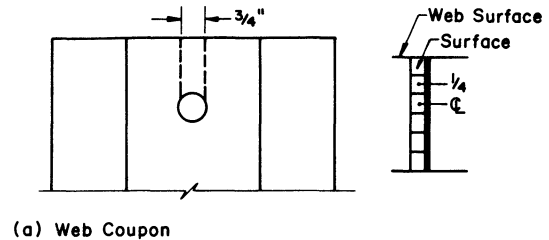
Fig. 15. Charpy V-Notch test results for $W14 \times 370$ section—Supplier A

energy. Few of these specimens were less than 20 ft-lbs. down to 32° F. Hence, the outer skin of the section had adequate levels of absorbed energy for welded surface attachments and shallow discontinuities.

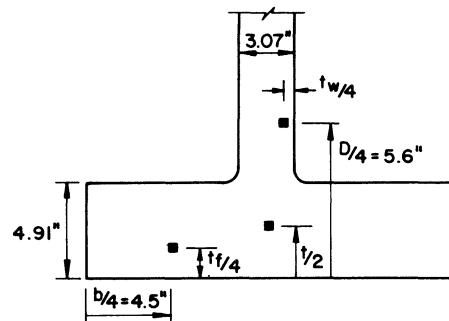
The characteristics of the $W14 \times 730$ sections shown in Figs. 3 and 4 were also examined. The only material available from these sections was a small segment cut between the end of the section and a lifting hole, as in Fig. 16a. The CVN specimens adjacent to the web surfaces had their notches extending 0.5 in. into the web. Hence, no shallow surface notches were examined. Several tests were also available on other sections tested by the manufacturer. These specimens were at the quarter thickness of the web and flange and at the center of the flange as sketched in Fig. 16b.

Test results for web specimens fabricated from the small segment shown in Fig. 16 are plotted in Fig. 17. The specimens were tested at 40° F, 70° F and 100° F. These test results are shown as solid and open dots and a cross. The tests by the manufacturer were only carried out at 100° F. The test results can be seen to be similar to the absorbed energy provided by the $W14 \times 370$ section plotted in Fig. 15. One side of the web surface provided higher levels of energy than its companion on the other side.

The test results indicate that providing steel to killed fine-grain practice has not resulted in a significantly higher level of absorbed energy for this $W14 \times 730$ section. Its level of absorbed energy is nearly identical to the $W14 \times 370$ section that was not furnished as killed steel. Additional tests carried out on $W14 \times 550$, $W14 \times 605$ and $W14 \times 730$ A572 steel sections were limited to segments cut from the web, shown schematically in Fig. 18. The surface layer specimens were notched so that the notch tip was within 0.25 in. of the web surface. The other speci-



(a) Web Coupon



(b) Location of CVN Specimens

Fig. 16. Schematic showing CVN test specimen locations for $W14 \times 730$ sections—Supplier B

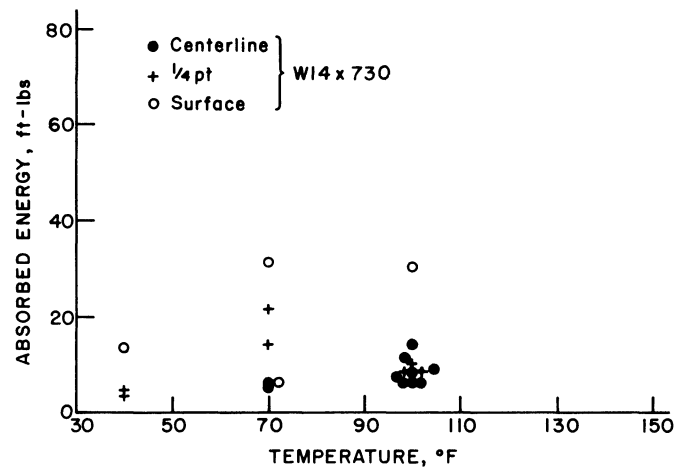


Fig. 17. Charpy V-notch test results for $W14 \times 730$ section—Supplier B

mens were near the 1/4 point and the centerline. The test results are plotted in Figs. 19, 20 and 21 for the three section sizes. It can be seen that the centerline of each of the web sections examined were not much different than the $W14 \times 370$ and $W14 \times 730$ sections shown in Figs. 15 and 17. The results from the $W14 \times 605$ section were lower at one end than at the other. However, both ends fell within the scatterband provided by the $W14 \times 370$ section.

d. Fracture Toughness, K_c

Compact tension specimens were fabricated from the flanges of the $W14 \times 370$ section in Fig. 1 and the web segments sketched in Fig. 18 for the $W14 \times 550$, $W14 \times 605$ and $W14 \times 730$ sections. Each flange specimen was cen-

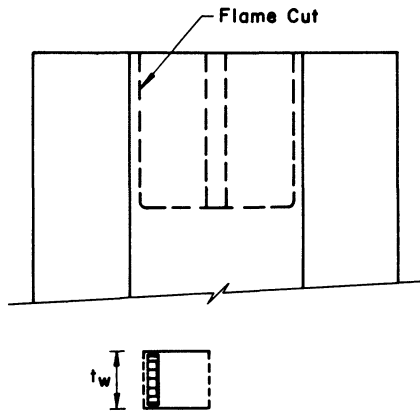


Fig. 18. Schematic showing location of web samples removed from sections—Supplier C

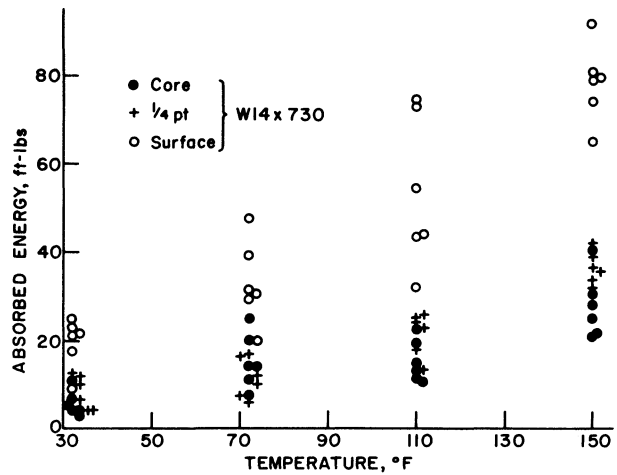


Fig. 21. Charpy V-notch test results from web of W14 x 730 section—Supplier C

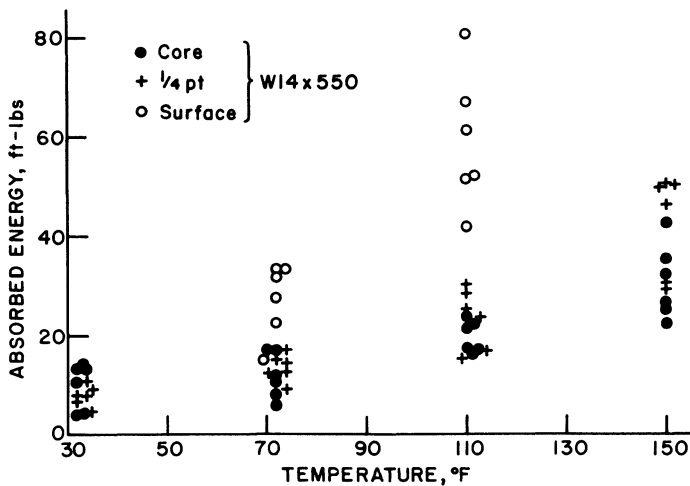


Fig. 19. Charpy V-notch test results from web of W14 x 550 section—Supplier C

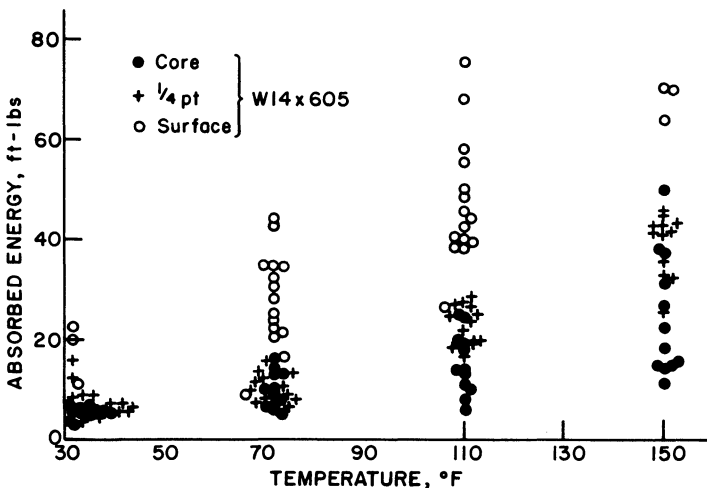


Fig. 20. Charpy V-notch test results from web of W14 x 605 section—Supplier C

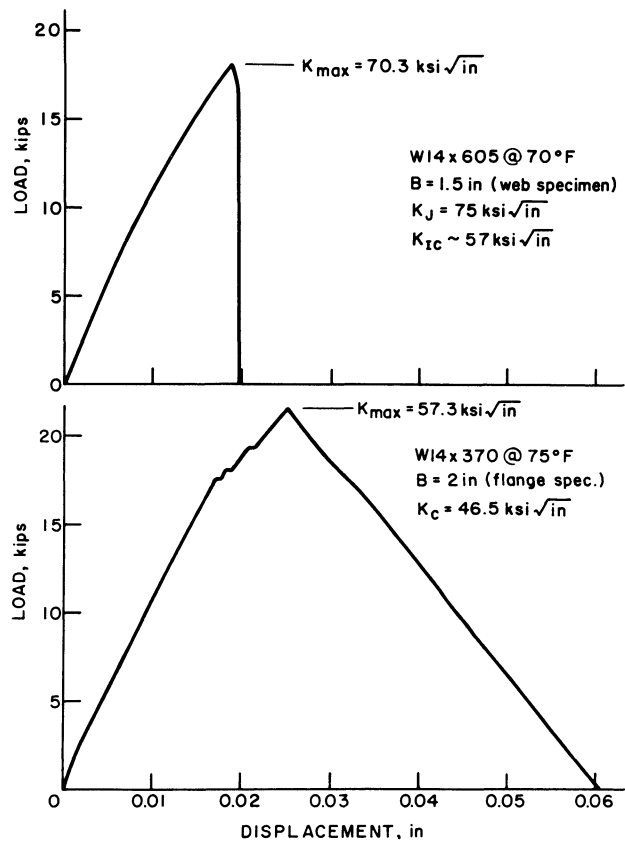


Fig. 22. Load-deflection curves for compact tension specimens from W14 x 370 section (Supplier A) and W14 x 730 section (Supplier C)

tered on the flange thickness and was 2 in. thick. The specimens fabricated from the web samples for the W14 x 550, W14 x 605 and W14 x 730 sections were centered on the web and were 1.5 in. thick, because available material was limited. All specimens were fabricated in accord with ASTM Specification E399 and tested at a static loading rate.

Figure 22 shows the load-deflection curve obtained for

tests carried out at 75° F on the W14 × 370 flange and the W14 × 605 web. The load-deflection plot for the flange was typical for all tests carried out on the west beam section in Fig. 2. Linear behavior was experienced throughout the tests of the W14 × 370 section specimen. An initial pop-in crack was heard at a stress intensity level of 34.2 ksi √in. As is apparent, several other crack advances were observed before final failure. The 5% secant offset suggests a fracture toughness K_{Ic} (static) of 46.5 ksi √in. It is apparent the fracture toughness for the service temperature corresponding to failure is about 45 ksi √in. for the W14 × 370 section in Fig. 23.

The W14 × 605 section results plotted in Fig. 23 exhibited minor inelastic behavior before fracture. K_{max} (based on P_{max}) provides a fracture toughness estimate of 70 ksi √in. The K_J estimate considering the nonlinear load-deflection response increased the estimated resistance to 75 ksi √in. The 1-½ in. thick specimen did not satisfy the requirements of E399 for plane strain, i.e.

$$t \geq 2.5 \left(\frac{K}{\sigma_y} \right)^2 \quad (1)$$

This would have required a thickness approaching that of the flange. As noted, there was not enough material available for full web thickness tests. Hence, the test results

from the 1-½ in. specimens are an overestimate of the actual fracture toughness of the flange material if its absorbed energy were identical to the web.

Figure 24 compares the fracture surfaces of the 75° F fracture tests from the W14 × 370 and W14 × 605 shapes. It is apparent crack surfaces show little evidence of ductility. The surface of the W14 × 370 specimen is comparable to the final fracture appearance of the cracked beam flange in Fig. 6. It can be seen that once fracture initiated in the W14 × 605 section that it also exhibited a cleavage fracture appearance over the crack surface.

For structural steels in the transition temperature range, the degree of plane strain restraint has a strong influence upon the test results. Because of the convenience of small specimen tests, considerable attention has been given to empirical methods which permit estimates of K_{Ic} values from small specimen results. Irwin has suggested an adjustment using the relationships.⁵

$$K_c^2 = K_{Ic}^2 (1 + 1.4 \beta_{Ic}^2) \quad (2)$$

where

$$\beta_{Ic} = \frac{1}{B} \left(\frac{K_{Ic}}{\sigma_y} \right)^2 \text{ and } \beta_c = \frac{1}{B} \left(\frac{K_c}{\sigma_y} \right)^2 \quad (3)$$

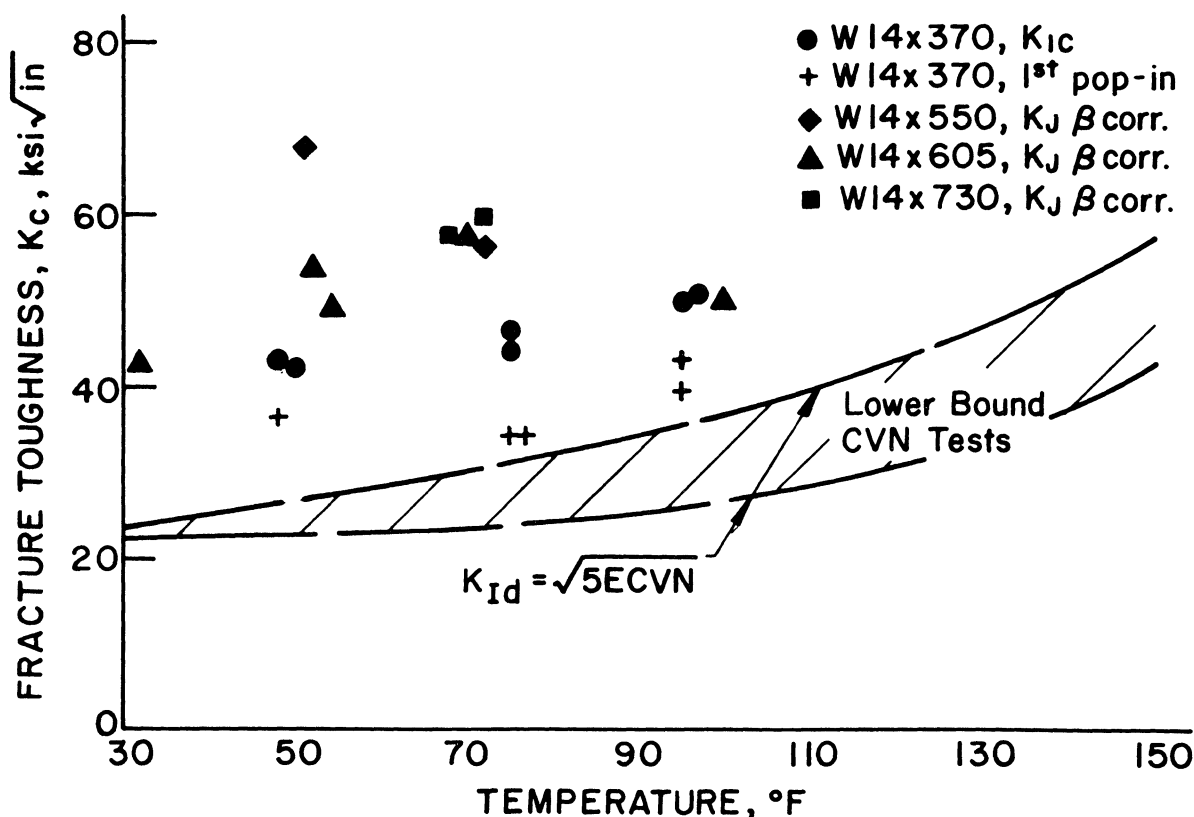
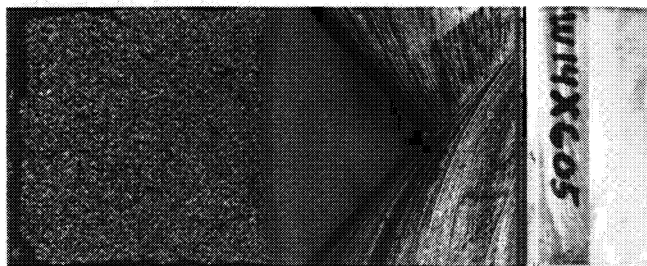


Fig. 23. Comparison of static K_c test results with lower bound Charpy V-notch estimate (dynamic)



(a). Fracture surface of compact tension specimen from flange (see Fig. 22. W14 x 370)



(b). Fracture surface of compact tension specimen from web (see Fig. 22. W14 x 730)

Fig. 24. Fracture surfaces of K_{Ic} specimens showing cleavage fracture at 70° F

B is the test specimen thickness and σ_y , the yield point of the steel. Use of these equations to estimate K_{Ic} for a thick section (high constraint) in service applications has been found to give appropriate values in several applications.^{5,6}

In this study, it was not feasible to make full plate thickness fracture specimens. The web thickness varied from 2.38 in. (W14 x 550) to 3.07 in. (W14 x 730) and the corresponding flange thickness from 3.82 in. to 4.91 in. Estimates of the K_{Ic} toughness values, which would be expected to control the onset of cleavage fracturing in the heavy flanges were made using Eqs. 2 and 3 to correct for the 1.5 in. specimen test results for the influence of constraint.

Figure 23 summarizes the test results and also shows the estimated dynamic fracture toughness K_{Id} , based on the relationship:

$$K_{Id} = (5 ECVN)^{1/2} \quad (4)$$

where K_{Id} is psi $\sqrt{\text{in.}}$, E is the elastic modulus in psi and CVN is ft-lbs of absorbed energy. This relationship is frequently referred to as the Barsom correlation equation.³ It can be seen from Fig. 23 the fracture toughness between 50° and 100° F varies between 40 ksi $\sqrt{\text{in.}}$ and 60 ksi $\sqrt{\text{in.}}$ for all five sections examined.

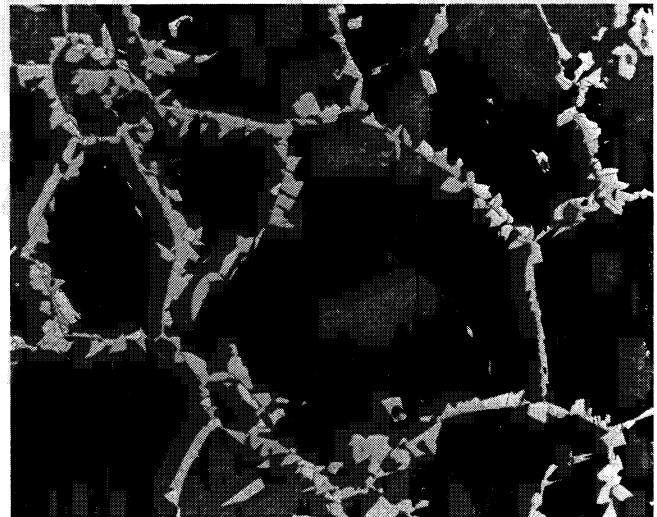


Fig. 25. Microstructure near flange core crack in Fig. 11. @ 100x (W14 x 370)—Supplier A

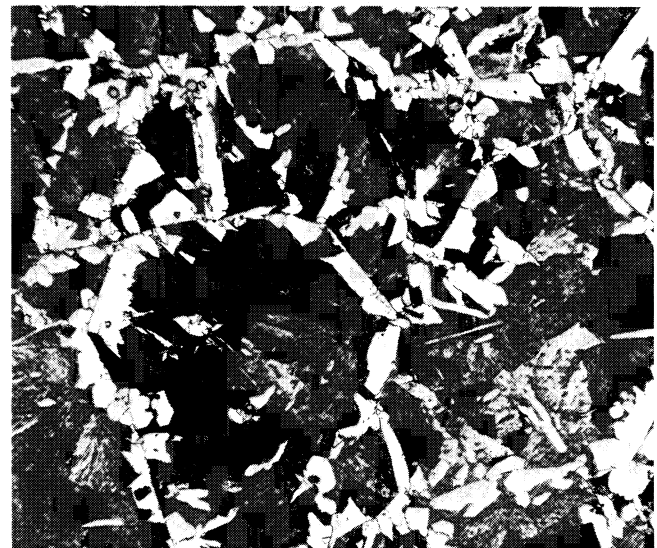


Fig. 26. Microstructure of fractured flange shown in Fig. 6. @ 100x (W14 x 370)—Supplier A

e. Metallographic Characteristics of the Core

The metallographic characteristics of the sections examined in this paper are reviewed in this section. This includes the core regions of the two W14 x 370 sections on each side of the groove weld in Fig. 2, the web of the W14 x 370 section in Fig. 3 and the webs of the other three sections examined in this chapter.

Figure 25 shows the microstructure of the W14 x 370 section just behind the crack surface in Fig. 6. The ASTM prior austenite grain size (ASTM E112) is between 0 and 1 for the 100x photomicrograph. Figure 26 shows the microstructure adjacent to the crack in the core area in Fig. 9. This also indicated the grain size in the web-flange core

region was between ASTM 0 and 1. Hence, the two W14 × 370 sections connected by the groove-welded splices had comparable metallographic characteristics. The section removed from the web of the W14 × 730 section, shown schematically in Fig. 16, exhibited similar characteristics. Figure 27 is a photomicrograph of the web centerline @ 100x. The prior austenite grain size is between ASTM 1 and 2. A cylindrical core removed from the web-flange core area provided an ASTM grain size of 0. Hence, the killed-steel W14 × 730 sections provided essentially the same prior austenite grain size characteristics as the W14 × 370 sections in Figs. 25 and 26.

The microstructure of the three sections examined from Supplier C are shown in Figs. 28, 29 and 30. The photomicrographs show the grain structure at the web centerline near the quarter depth of the section. The evaluation of grain size in these steels is more complex than might appear. The microstructure of these steels contains two constituents. Light etching nearly pure iron (ferrite) and dark etching iron-iron carbide mixtures (pearlite). These two regions are seen in Fig. 28, where the ferrite grain size is most readily seen. It is the size of the white-appearing grains that surround the darker pearlite regions. This is *not* the grain size referred to in “fine-grain practice.” Rather, it is the austenite grain size existing at high temperatures prior to transformation to ferrite and pearlite. Prior austenite grain size is difficult to evaluate in low-carbon steels because the low temperature products, ferrite and pearlite obscure it. It is evaluated using ASTM specifications which involve heating the steel to a temperature below that at which the steel is usually finished (1,750 °F) followed by slow cooling. This is called the McQuaid-EHN Test. When a steel is finished in normal rolling practice, it may not actually have a fine prior austenite grain size that it has in the McQuaid-EHN Test, especially in the heavy sections.

What “fine-grain practice,” in fact, means is that the steel supplier uses aluminum as a deoxidant so the fine-grain size will result *if the proper heat treatment is used*. To have fine prior austenite grain size in the steel, then it must be normalized, that is, heat treated at 1,750° F followed by air cooling like the McQuaid-EHN specimen. To have assured fine-grain *size* steel in contrast to fine-grain *practice* steel, both aluminum deoxidation and normalizing heat treatment must be done. For these structural shapes, this rarely happens. For heavier sections considered in this application, not only are the finishing temperatures high (over 2,000° F), but also the amount of mechanical deformation at the flange-web core is small. A lack of extensive hot deformation leaves the cast ingot structure unrefined. This condition, along with high finishing temperatures, usually leads to coarse, low toughness steel at the flange-web intersection regardless of deoxidation practice.

If the pearlite content is unusually high, the prior austenite grain size can be seen. This is the case in Figs. 25 and 26, and to a lesser extent in Fig. 30. The prior austenite grain sizes in both these cases, one of which is a fine-grain prac-

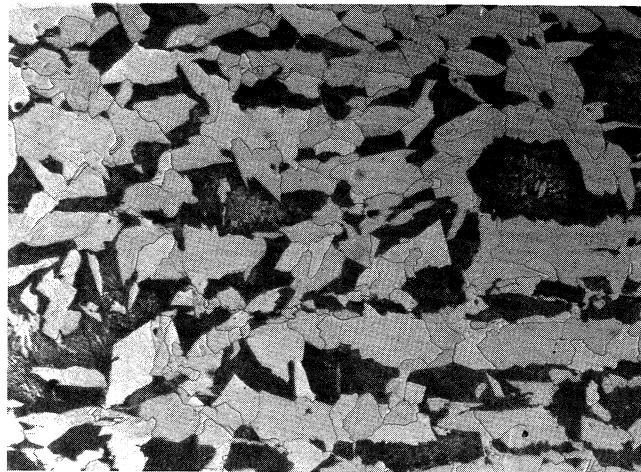
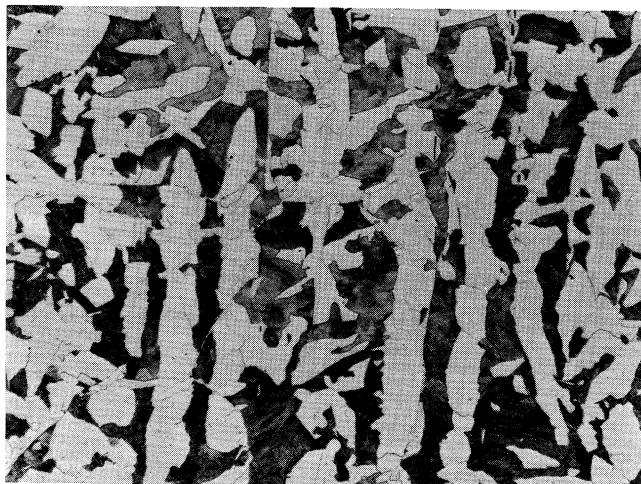
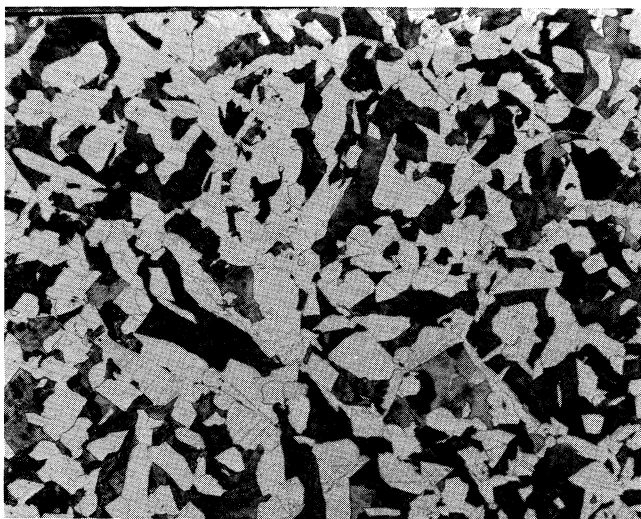


Fig. 27. Microstructure of web centerline (see Fig. 16.) @ 100x (W14 × 730)—Supplier B



(a). Web centerline @ 100x

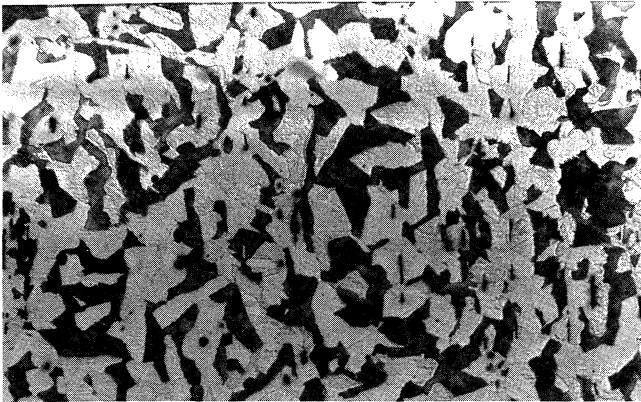


(b). Web surface @ 100x

Fig. 28. Microstructure of web—W14 × 550—Supplier C



(a). Web centerline @ 100x



(b). Web surface @ 100x

Fig. 29. Microstructure of web—W14 × 605—Supplier C

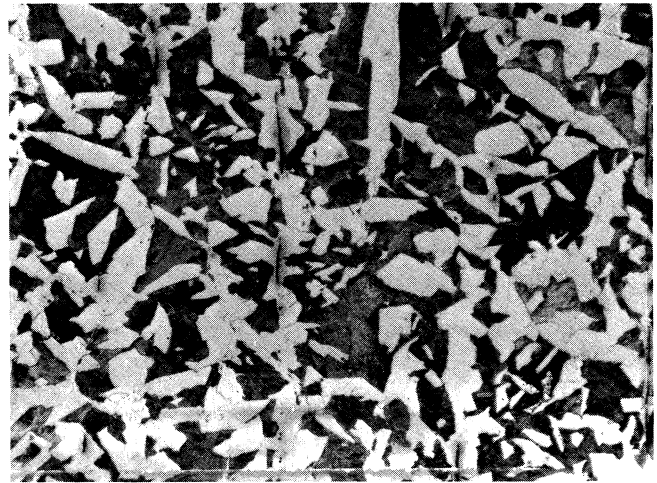
tice steel (Fig. 29a), is large. Thus, fine-grain practice had little effect here.

Grain size is rated on an ASTM scale from 0 to 10, 0-5 being coarse, 6-10 being fine. As indicated, these steels rate from 0-1 and are coarse grained.

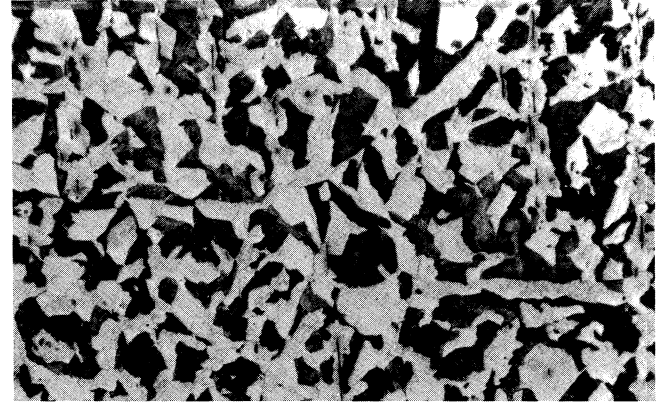
EVALUATION OF FRACTURES

a. Fracture of the Truss Member

The crack surface of the W14 × 370 section from the truss in Fig. 2 is visible in Fig. 6. A dark, oxide-covered region can be seen in Fig. 6b at the core of the web-flange intersection. In general, the crack surface shows a flat cleavage appearance. Some small shear lips are apparent at the flange tips and the bottom surface of the flange. The dark oxide surface in Fig. 6b is the size of the initial crack that existed at the failure cross section. This crack extended 1.15 in. from the edge of the cope into the flange. Its maximum width was 2.75 in.



(a). Web centerline @ 100x



(b). Web surface @ 100x

Fig. 30. Microstructure of web W14 × 730—Supplier C

The fracture surfaces of the flanges were examined with particular focus on the large initial crack condition in Fig. 6. Surface replicas for study in the transmission electron microscope (TEM) were obtained. In addition, the fracture surface was cut into smaller segments to permit direct examination in the scanning electron microscope (SEM).

Figures 31 and 32 are fractographs of the darker oxide covered region. Figure 31 (at 200x) shows oxidation, corrosion product and some evidence of cleavage facets. Figure 32, with a higher magnification (2,000x), shows a cleavage facet and some evidence of corrosion. Figure 33 is a view of the cleaner appearing fracture surface that existed over most of the fracture surface. The photomicrograph, adjacent to the darker region, shows fresh fracture with clear cleavage facets. A comparison of Figs. 31 to 33 indicates the darker, oxide-covered fracture region existed for some period of time prior to the final fracture.

The fractographic examination of the crack surface, the observations on the crack detected in the east beam at the

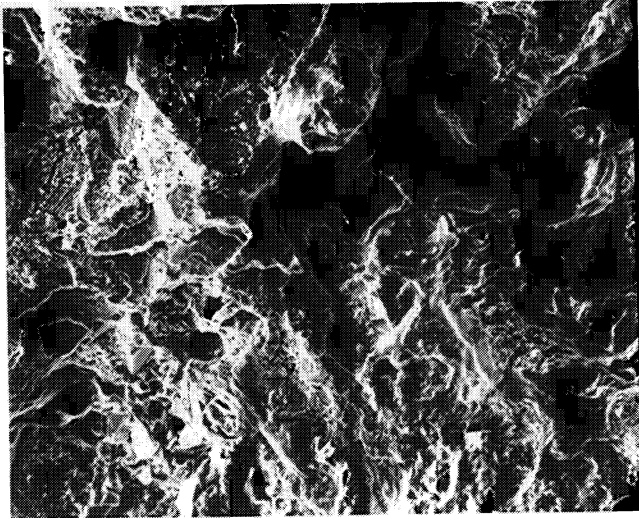


Fig. 31. Fractograph of the dark oxide region shown in Fig. 6. showing oxidation, corrosion and cleavage facets @ 200x

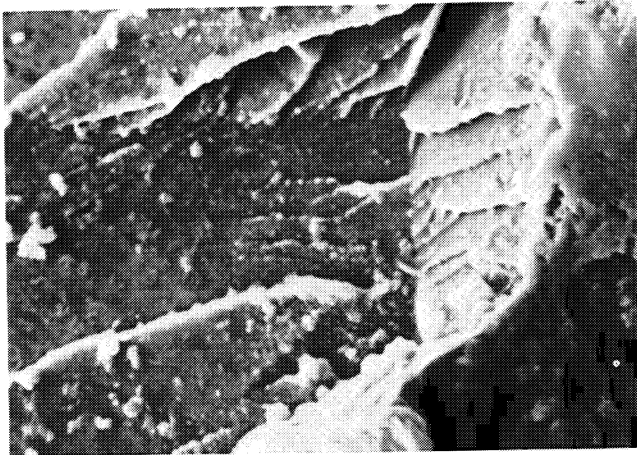


Fig. 32. View of region shown in Fig. 31. @ 2,000x



Fig. 33. Fractograph of clean fracture area in Fig. 6 @ 100x showing cleavage facets

south flange cope and the material fracture toughness results can be used to establish the expected crack extension behavior of the web-flange core and the final fracture of the chord shown in Fig. 1. This section provides an analysis of the crack development.

1. Formation of initial cracks in the flange copes

Of major importance to the formation of the large initial crack observed on the fracture surface (Fig. 6) was the high stress concentration provided by the flame-cut cope, the low fracture toughness of the beam and the stresses from groove welding the two heavy rolled sections together. The groove welds in the web and flanges at shop splices were prepared as follows. First, the beveled ends were fitted up with about 1/8-in. gap and with the flanges vertical. Root passes were made on both flanges with E7018 electrodes to hold the sections together. The top half of the web groove weld was completed, and then the section was turned over, and the web weld was completed. The section was then turned 90°, and the outside half of a flange weld was completed. The second flange weld was also made on the outside half. Finally, the inside weld halves of the flanges were completed.

The result of this weld sequence is that final weld passes are highly restrained against longitudinal shrinkage along the member axis. As a result, the final flange closure results in at least yield point residual stress in the interior half of the flange. The resulting stress introduced into the flame-cut cope is at least 60 ksi. The flame-cut cope can be modeled as an edge crack in a stress gradient region. The stress intensity factor for this condition is

$$K = 1.12 F_g \sigma_y \sqrt{\pi a} \quad (5)$$

where

$$\sigma_y = \text{yield point} = 60 \text{ ksi}$$

$$F_g = \text{stress gradient correction for the flame-cut notch} \sim 1.5$$

$$a = \text{initial crack size} = 0.06 \text{ in.}$$

Hence, K at completion of the weld is

$$K = 1.12 (60) (1.5) \sqrt{\pi 0.06} = 44 \text{ ksi} \sqrt{\text{in.}} \quad (6)$$

This level of stress intensity factor exceeds the fracture toughness of the web-flange core of the W14 × 370 section shown in Fig. 23. As a result, crack propagation occurs and the initial crack condition that existed in the flange copes is inevitable.

The resulting crack instability will arrest when the crack enlarges and releases the residual stress field and moves into a lower stressed or higher toughness region. For crack arrest, the stress intensity factor must decrease below the dynamic fracture resistance of the flange material. As seen in Fig. 23, this value is about 30 ksi $\sqrt{\text{in.}}$ based on the Barsom correlation equation. An estimate of the remaining residual stress can be made by equating the resulting stress intensity factor to the dynamic fracture resistance. The

applicable stress intensity factor is provided by a circumscribed circular shaped crack.⁴ The K value is

$$K = \frac{2}{\pi} \sigma_r \sqrt{\pi a_1} \quad (7)$$

where

a_1 = radius of the circumscribed crack ~ 1.125 in.

σ_r = residual stress

Equating Eq. 7 to 30 ksi $\sqrt{\text{in.}}$ provides an estimate of residual stress equal to about 24 ksi. This is the condition that exists as trusses are erected in the field and dead load added during construction.

2. Final fracture of the chord

The estimated additional stress in the chord during construction was about 11 ksi. Hence, at fracture the stress intensity factor was equal to

$$K = \frac{2}{\pi} (24 + 11) \sqrt{\pi (1.25)} \quad (8)$$

$$= 44.2 \text{ ksi } \sqrt{\text{in.}}$$

This again equals the fracture resistance of the low toughness beam and results in brittle fracture. The balance of the section failed at the same time. This level of stress intensity is below the fracture resistance of the adjacent higher toughness beam, and hence, the crack in that beam was not critical at the time of the failure.

b. Cracking of the Column Web

The cracks formed in the column webs in Figs. 3 and 4, result from the low level of fracture toughness in the core and adjacent web centerline and the high residual stresses from weld shrinkage. The joint configuration insures the web weld terminates in a region of low fracture toughness. The resulting transverse and longitudinal weld shrinkage insures that this region is at the yield point. The stress intensity at the weld end can be defined

$$K = 1.12 \sigma \sqrt{\pi a} \quad (9)$$

Since the yield point of the section is 61.7 ksi, and the estimated fracture toughness K_{Ic} of the core and web centerline is about 35 ksi $\sqrt{\text{in.}}$ at 20 to 40° F, Eq. 9 can be equated to K_{Ic} as:

$$1.12 (61.7) \sqrt{\pi a_{cr}} = 35 \text{ ksi } \sqrt{\text{in.}} \quad (10)$$

This yields $a_{cr} = 0.1$ in.

Considering the termination conditions existing at the end of the web-groove weld, fracture occurs and the crack propagates following the principal tensile stress field. The cracking relieves the high restraint stresses and this assists in crack arrest. Many of the cracks arrested when they encountered the lifting hole or else propagated until they intersected the unfused plane at the ends of the column

flanges. For the crack in Fig. 4, it is probable an internal defect near the fusion line initiated crack instability. The stress intensity factor for this condition can be approximated as

$$K = \frac{2}{\pi} \sigma_y \sqrt{\pi a} \quad (11)$$

where

a is the radius of the circumscribed defect. This yields

$$\frac{2}{\pi} (61.7) \sqrt{\pi a_{cr}} = 35 \text{ ksi } \sqrt{\text{in.}} \quad (12)$$

and $a_{cr} = 0.253$ in.

This corresponds to the size of discontinuities permitted in such large thickness components.

It does not seem advisable to provide web-groove welds (partial or full penetration) that terminate in or are adjacent to the web core. Since milled surfaces usually exist, it is impossible to provide web-groove welds without significant levels of residual stress. Hence, the possibility of initiating crack instability will be great. Whatever shear or load transfer that is required from the web should be accomplished by using splice plates fillet-welded to either the web surface away from the core or the flange tips.

c. Cracks from Flame-cut Edges

Cracks originating from a flame-cut edge (as in Fig. 5) are oriented in an even lower notch sensitive area. Charpy V-notch tests with a transverse-longitudinal orientation (TL) are in Fig. 34. As can be seen, the absorbed energy is between 1 and 5 ft-lbs. up to 212° F. Hence, lower bound fracture toughness of about 20 ksi $\sqrt{\text{in.}}$ appears appropriate for this orientation.

The stress intensity for the flame-cut edge can be taken as

$$K = 1.12 \sigma \sqrt{\pi a} \quad (13)$$

Since flame-cutting will often produce a brittle untempered martensite layer about 0.025-in. thick, as in Fig. 11, this can

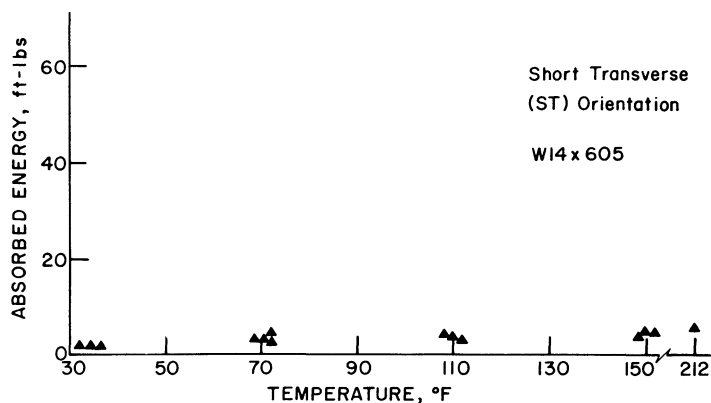


Fig. 34. Charpy V-notch tests in the short transverse direction (notch parallel to axis of shape) W14 x 605 section

be assumed as the initial crack size. Equating Eq. 13 to the lower bound toughness yields

$$1.12 \sigma \sqrt{\pi(0.025)} = 20 \text{ ksi } \sqrt{\text{in.}} \quad (14)$$

This indicates the yield stress σ_y will initiate crack extension into the section. These cracks will arrest as they extend out of the residual tensile stress region. Noted earlier, this type of crack was observed to extend 0.5 to 0.75 in. into the shape before arresting.

CONCLUSIONS AND RECOMMENDATIONS

The web-flange core and the center of the web adjacent to it for heavy jumbo sections was found to provide Charpy V-notch values between 3 and 10 ft-lbs. up to 100° F. Even at 150° F, values were only 10-20 ft-lbs. for many sections. Fracture toughness tests were also carried out and demonstrated the static fracture toughness K_{Ic} was between 40 and 60 ksi $\sqrt{\text{in.}}$ at temperatures between 50-100° F.

The core area was found to possess a coarse prior austenite grain structure. The grain size in the core and web center adjacent to it was found to be between ASTM 0 and 1. The surface layers were always found to be very tough. These characteristics appear to be typical for many jumbo sections. The core area and adjacent web does not get worked in the jumbo section during the rolling process to the degree that smaller sections do. It has a "cast-like" structure and inherently less fracture toughness. The surface layers receive more work and deformation, and this refines the grain structure and enhances their fracture toughness properties.

With the low fracture toughness core, the notches provided by flame-cut access copes, and the high residual stresses from groove welded splices, cracks are likely to

form during fabrication. Although carefully ground copes will improve the surface notch condition, inadequate margins of safety will still result at normal welding discontinuities near the fusion line. Hence, groove welded splices should not be used in tension applications with heavy jumbo sections. Bolted connections should be used for tension member splices. This will avoid introducing high residual stresses, sharp notches and flaws into the section.

Welded attachments should be limited to the surfaces of jumbo sections where significantly higher fracture resistance exists. This permits surface welds to be made without introducing adverse conditions at the fusion line and weld termination. All welding processes result in nonmetallic microdiscontinuities at the toes of groove and fillet welds. These will have no significance for static behavior with the levels of absorbed energy in the surface layer of all the sections examined. Surface welds will not result in the embedment of these discontinuities into the material that is very notch sensitive. As a result, loads applied through exterior welded attachments will not be affected by the interior grain structure and notch sensitive material. This has been demonstrated in many service applications, including trusses shown in Fig. 1.

Care should be exercised in the use of groove welded web splices in column sections. It would be preferable to use fillet-welded shear plates attached to the section surface or a bolted shear splice, as in Fig. 35.

When flame-cutting large jumbo sections, care needs to be exercised to prevent the formation of brittle untempered martensite. This can be minimized with preheat and post-heat treatment. Fortunately, the longitudinal cracks that form are in a favorable orientation parallel to the stress field and have little effect on the performance of the member.

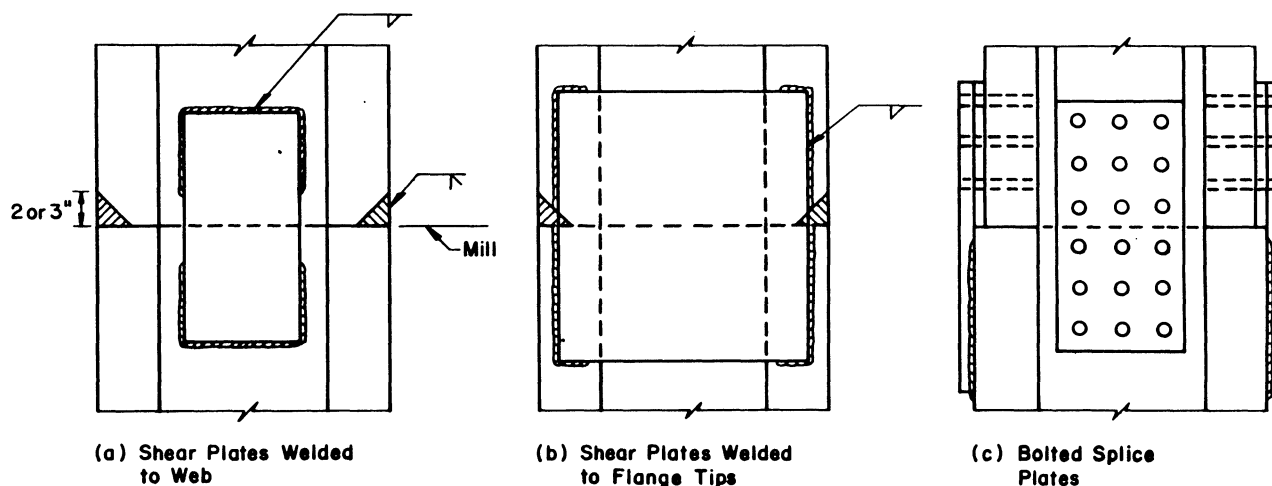


Fig. 35. Alternative column splices that minimize weld restraint tensile stresses

ACKNOWLEDGMENTS

This paper is based on studies of several cases of cracking that developed during construction. The authors are indebted to the Orange County Civic Center and Orange County Attorney, G. H. Harris, the Atlas Iron Works and to Stanley Goldstein, P.C., and Neal S. Moreton, Inc. for providing details and information.

Thanks are also due Prof. G. R. Irwin for assistance and suggestions, and to Drs. B. R. Somers and E. J. Kaufmann for assisting with the material tests and metallographic studies. Thanks are also due R. N. Sopko for photographic assistance, Mrs. Sharon Balogh for preparation of the figures and Mrs. Ruth Grimes for typing the manuscript.

REFERENCES

1. *American Institute of Steel Construction, Inc. Manual of Steel Construction 8th Ed., 1980, Chicago, Ill.*
2. *Alpsten, G. A. and L. Tall Residual Stresses in Heavy Welded Shapes Welding Journal, Vol. 49, March 1970.*
3. *Rolfe, S. T. and J. M. Barsom Fracture and Fatigue Control in Structures Prentice-Hall, 1977.*
4. *Fisher, J. W. Fatigue and Fracture in Steel Bridges Wiley Interscience, 1984, New York, N.Y.*
5. *Irwin, G. R. Linear Fracture Mechanics—Fracture Transition and Fracture Control Engineering Fracture Mechanics, Vol. 1, 1968 (pp. 241–257).*
6. *Merkle, J. Construction Research for Materials Engineering Branch U.S. Nuclear Regulatory Commission Report #NUREG-0975, Vol. 1, March 1983.*